Proceedings of the Thirty-third (2023) International Ocean and Polar Engineering Conference **www.isope.org**
Ottawa, Canada, June 19-23, 2023
Copyright © 2023 by the International Society of Offshore and Polar Engineers (ISOPE)
ISBN 978-1-880653-80-7; ISSN 1098-6189

Numerical Analysis of In-service Welding Carried out Using GMAW Process Assisted by Induction Heating

Kaue Correa Riffel[1], Regis Henrique Gonçalves e Silva[1], Antonio Jose Ramirez Londono[2], Marcelo Torres Piza Paes[3], Jair Carlos Dutra[1]
[1]Federal University of Santa Catarina, Florianopolis, Santa Catarina, Brazil.
[2]The Ohio State University, Columbus, Ohio, USA
[3]Petrobras/CENPES, Rio de Janeiro, Brazil

ABSTRACT

This paper presents an approach to simulate the in-service welding of type-B sleeves using finite element analysis (FEA) and induction preheating. To validate the models, numerical results of thermal cycles and temperature distribution are compared with experimental data. The maximum error in the tail out of the thermal cycles (cooling slope) was about 10%, while in the peak temperature, the error was about 5%. The cooling time between 800 ºC and 500 ºC ($\Delta t_{8\text{-}5}$) was also estimated and the microstructure was predicted using continuous cooling transformation (CCT) diagrams.

KEY WORDS: Welding simulation; Finite element analysis; repair welding; Thermographic monitoring; High cooling rate welding.

INTRODUCTION

In-service welding is a repair technique applied in the oil and gas industry. In-service welding demand has increased in the Brazilian scenario in the last few years due to corrosion, vandalism, and fuel theft. Some examples of in-service applications are type-B sleeves, patches, welding overlay, and fittings for hot-tapping (Bruce, 2002). One of the main issues in such a technique is the faster cooling rate compared to conventional welding. The repaired part can be filled with inflammable liquids, or gases, with or without flow and high pressure can be an extra difficulty. High cooling rates make the welding heat-affected zone (HAZ) prone to brittle microstructures and hydrogen-induced cracking (HIC) (Bruce and Bradley, 2012). Depending on the welding process heat input the blowout/burn-through risk is also a concern because the weld pool can act like a stress concentrator and the temperature rising of the wall can reduce the yield stress of the component, increasing the defect susceptibility (Sabapathy et al., 2000; Boring and Bruce, 2008). With the numerous parameters involved in the welding of equipment in operation, it is very important to control the variables and the part conditions before the welding is carried out.

The welding procedure qualification is assembled by mounting complex systems with water circulation according to API 1104 (2007). Experimental tests, highlighted in the standard, aim to reproduce great thermal severity and ensure that the welding is qualified to be applied in real cases (Guest et al., 2016; Yunovich and Thompson, 2005).

Regarding the HIC susceptibility, pre-heating is a technique capable of reducing the cooling rate of the welding, facilitating phenomena like hydrogen diffusion out of the part and in some cases even the precipitation of more ductile microphases (Lippold, 2014; Kou, 2003). Due to the thermal severity sometimes faced in in-service welding common pre-heating methods (flame and resistance) are not applicable due to the low thermal efficiency and the low temperature reached in the part (Korol'kov, 2012). Thus, the use of methods for the estimation of the part condition as a function of certain parameters is a tool that enables an understanding of physical phenomena that are difficult to measure during an in-service welding procedure.

Predicting results can be performed numerically using methods like finite elements analysis (FEA). In-service welding FEA was previously applied in previous research to predict temperature for non-preheated parts. However, many effects and great errors between the experimental and simulated thermal cycles are verified, either due to physics simplifications or the leak of some phenomena consideration (Christensen et al., 1995; Goldak et al., 1984). Commercial software, for example, does not take into account the effect of preheating the part, nor the undeveloped flow existing in most of the cases of qualifications for in-service welding (Kiefner et al., 1981; Kiefner et al., 1983). The approach considered by the literature ignores the existence of complex multiphysics in the process, ending up ignoring many of the important variables that exist in an in-service application. The consequences are relatively large errors and an underestimation of the temperature, thermal cycles, and cooling rates of the welding (Ahmed et al., 2016; Wang et al., 2013).

This paper shows a multidisciplinary approach to simulate the in-service welding technique, aiming to present a FEA and a comparison with experimental results. In welding tests, a novel technique, the GMAW process with pulsed current (GMAW-P) and induction preheating, is applied to enhance the in-service welding reliability. GMAW-P is based on the rectangular waveform shown by Dutra et al. (2016) and Palani and Murugan (2006), in which the current varies between two levels (peak and background), and one droplet of molten material is deposited per cycle. GMAW-P can allow

more productivity and thermal input control, giving a greater parameterization range (Joseph et al., 2003; Bosworth, 1991).

Thus, this paper aims to present a multidisciplinary approach to the qualification, and temperature estimation of the in-service welding technique. The work includes multiphysics FEA and welding with novel techniques, as the GMAW-P assisted by induction preheating.

MATERIALS AND METHODS

A water loop was constructed to simulate in-service welding fast cooling. The sample was an API Grade B steel pipe with 324 mm (12.75 inches) in outside diameter and 9.5 mm (3/8 inches) thick. The water circuit can be seen in Fig. 1, which was composed of 2 m of steel pipe, a pump with 1.5 hp, a rotameter for water flow measurement, and a water reservoir. The water was kept at 20 ºC using a chiller connected to the reservoir and the flow rate was set to 380 l/min.

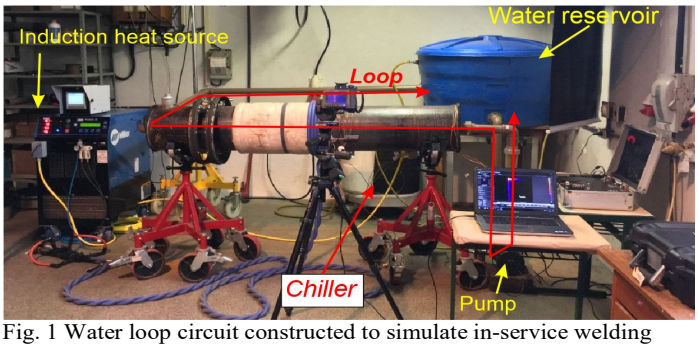

Fig. 1 Water loop circuit constructed to simulate in-service welding

The induction heating consists of water-cooled cables wrapped around the part. Two induction heat sources were used simultaneously to preheat the joint according to the schematic in Fig. 2. Such a configuration is named double heating, in which the joint is positioned between both coils in an accessible space of approximately 30 mm. A total of three welding beads were deposited to complete the circumferential joint.

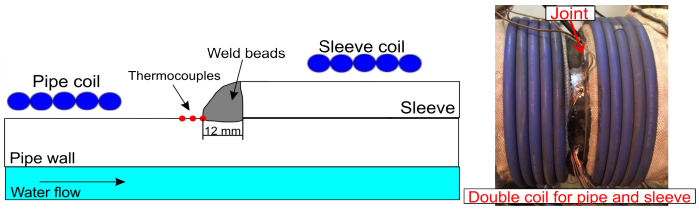

Fig. 2. Schematic of the type-B fillet joint and the coils set up

The methodology was based on the comparison of welding without preheating versus two preheated samples. In both cases, the maximum temperature hit in the sleeve was controlled at 400 ºC, while in the pipe two different temperatures were analyzed. In the first one, the temperature was about 90 ºC and in the second this value was increased to 200 ºC of preheating. Thus, 3 welding conditions were experimentally carried out and simulated in FEA:

1- Type-B sleeve welding without preheating;
2- Type-B sleeve welding with induction preheating (400ºC at sleeve and 90 ºC at pipe);
3- Type-B sleeve welding with induction preheating (400 ºC at sleeve and 200 ºC at pipe);

The filler metal used in the welding was an AWS ER 70S-6 with 1.2 mm in diameter and the shielding gas was a mixture of Ar+8%CO_2. The GMAW-P was parametrized in previous studies and can be seen in Table 1 (Riffel, 2022). The version chosen in this work is based on the rectangular waveform in Fig. 3. The current varies between a high (peak) and a low (background) level during a certain period (T) of time, which is divided into pulse time (t_p) and background time (t_b). Each T one droplet is detached from the tip of the filler metal approximately in the middle of the t_b, according to the schematic in Fig. 3.

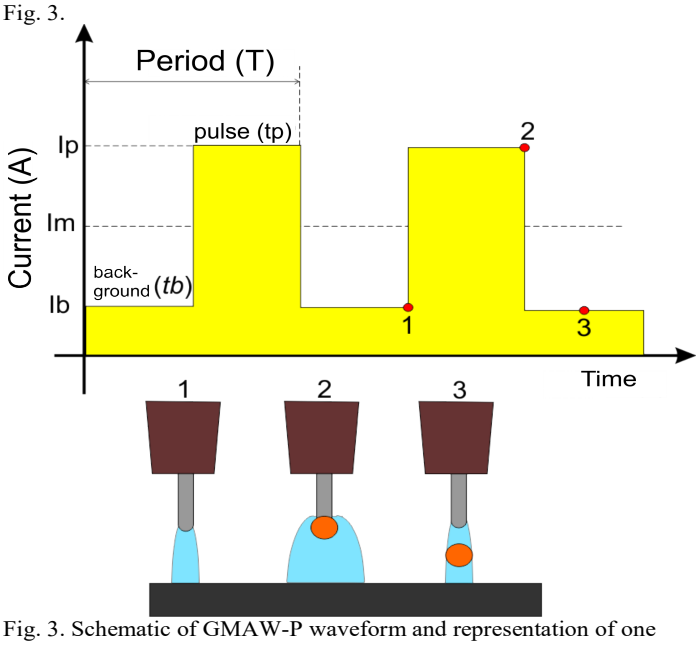

Fig. 3. Schematic of GMAW-P waveform and representation of one droplet per pulse

Table 1. Welding parameters applied to carry out the circumferential weld beads (Riffel, 2022)

Welding parameters of GMAW-P	
Pulse current (I_p)	380 A
Pulse time (t_p)	2.7 ms
Background current (I_b)	60 A
Background time (t_b)	3.5 ms
Average current (I_m)	200 A
Average voltage (U_m)	26.0 V
Average power (P_m)	6060 W
Wire feed speed (WFS)	6 m/min
Contact tip to work distance (CTWD)	17 mm
Travel speed (TS)	30 cm/min

The temperature was measured with type-K thermocouples using an IMC Portable Acquisition System (IMC Soldagem, 2023). They were attached to the pipe's surface close to the joint region, where the arc passes and the weld bead is formed. In order to ensure the measurement, three thermocouples were welded in the part. The first was 12 mm away from the joint followed by another two separated by 1 mm, according to Fig. 2.

Sequentially, the welded samples were characterized using

microhardness maps with a Leco modelo LM 100AT with a load of 200 g. The spacing between indentations was 150 µm as specified in ASTM E384 (2021). Microscopic characterization of the microstructure was carried out in a Leco model Olympus GX50 Inverted with 200X and 1000X magnification. The samples were prepared and etched using Nital 2%.

The last step of the chronological methodology was the creation of the models for simulation. A thermal analysis was carried out to evaluate the temperature distribution and the thermal cycle in the pipe, focusing on the cooling time between 800 ºC and 500 ºC ($\Delta t_{8\text{-}5}$). Fig. 4 shows the graphic interface of the software with the pipe modeled. A reduced geometry approach was applied in order to reduce the computational time. Thus the length of the model was 500 mm. The model was composed of 99074 tetrahedral elements, 0.62 of average quality (skewness) and 389188 degrees of freedom.

The FEM simulations were developed on COMSOL Multiphysics, applying the differential equations of the AC/DC and Heat transfer modules. The equations solved on the models are presented in Section 3. The computer setup was composed of a microprocessor AMD Ryzen 7 3800X with 8 cores and 16 threads, working at a clock frequency of 3.9 GHz, 64 Gb of RAM DDR4 of 2666 MHz, and an Adata SSD with 1 Tb of storage capability and reading/writing speed of 520/450 MB/s.

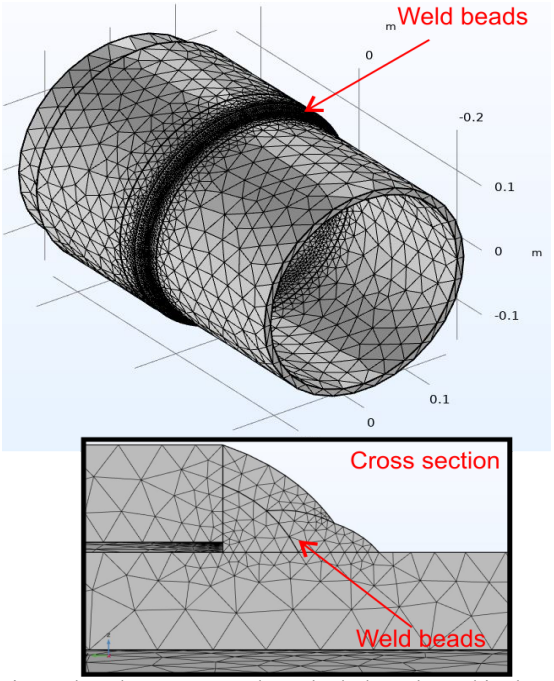

Fig. 4. Pipe-reduced geometry and tetrahedral mesh used in the simulation step.

Welding simulation and thermal analysis

The heat source of the welding process was considered using the double-ellipsoidal distribution. This volumetric heat source was presented by Goldak and Akklaghi, (2005) and is based on the Gaussian distribution. The mathematical model is composed of three semi-axis (a, b and c) parallel to the Cartesian axis (x, y and z).

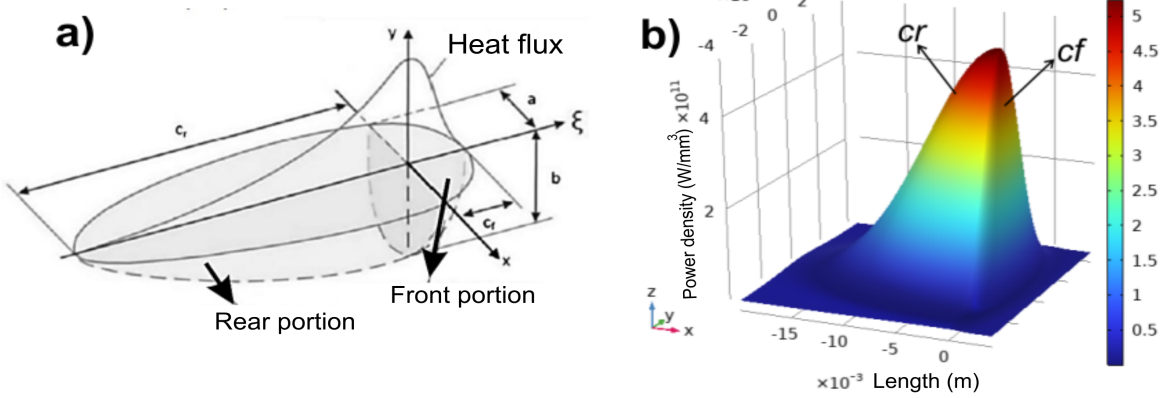

Fig. 5. In a) Double-ellipsoidal heat source; b) Heat density distribution.

The result is a profile divided into frontal and rear portions as presented in Fig. 5. The equations of the double-ellipsoid are presented in Eq. 1 and Eq. 2 and the sum of both equations is the total heat flux density. From the Fig. 5, it can be seen that the heat source is composed of geometrical input parameters based on the weld pool. The power distribution is described by both equations and a frontal fraction (f_f) and a rear fraction (f_r), besides the frontal length (c_f) and rear length (c_r).

$$q(x,y,z,t) = \frac{6\sqrt{3}f_f Q}{abc_f \pi\sqrt{\pi}} exp\left(-\frac{3x^2}{a^2}\right) exp\left(-\frac{3y^2}{b^2}\right) exp\left(-\frac{3[z+v(\tau-t)]^2}{c_f^2}\right) \quad (1)$$

$$q(x,y,z,t) = \frac{6\sqrt{3}f_r Q}{abc_r \pi\sqrt{\pi}} exp\left(-\frac{3x^2}{a^2}\right) exp\left(-\frac{3y^2}{b^2}\right) exp\left(-\frac{3[z+v(\tau-t)]^2}{c_r^2}\right) \quad (2)$$

Where, $f_f+f_r=2$; Ts is the welding speed, τ is a delay index used to set the position of the source at t=0; Q is the power of the electric arc, calculated by the multiplication of the welding current (I), voltage (U) and the process thermal efficiency (η).

From the thermal analysis, the model solved the energy balance Eq. 3 in its differential form to get the temperature in the part for a 3-D calculation. Thermal properties of the material are temperature dependent making the problem non-linear. The values

considered for the material's properties are presented in Table 2.

$$\left\{\frac{\partial}{\partial x}\left[k(T)\frac{\partial T}{\partial x}\right]+\frac{\partial}{\partial y}\left[k(T)\frac{\partial T}{\partial y}\right]+\frac{\partial}{\partial z}\left[k(T)\frac{\partial T}{\partial z}\right]\right\}+\dot{Q}(T,t)=\rho(T)C_p(T)\frac{\partial T}{\partial t} \quad (3)$$

Table 2. Carbon steel properties in function of the temperature applied to the simulation

Temperature/ Properties	20 ºC	300 ºC	500 ºC	700 ºC	1000 ºC	1500 ºC
k(W/(m*ºC))	55	48	45	34	30	35
C_p (J/(kg*ºC))	480	550	680	1000	640	825
ρ (kg/m^3)	8000	7900	7800	7700	7580	7150

The heat transfer coefficient (*h*) (boundary condition) considered on the internal surface was according to the approach applied by Riffel (2022), which simulated the fluid flow for an in-service welding qualification and found an average value of 3070 W/m^{2}K.

The second criterion evaluated for the validation of the FEA and the temperature distribution was the thermal cycles measured experimentally by thermocouples. For each pass (1, 2, and 3), only the maximum acquired temperature was used for comparison with the simulation. It is important to mention that sometimes the arc burned the thermocouples preventing the acquisition of higher temperature values. This is also an advantage of the simulation, once the model is calibrated, the temperature can be extrapolated to regions where the attachment of a thermocouple is difficult (e.g. near the molten zone and the arc path). Fig. 7 compares the measured curves versus calculated thermal cycles of the condition without preheating, in which an excellent agreement is verified between the curves. Dashed lines represent a ±10% error around the tail out of the measured temperature. Thus, it can be verified that the simulated cycles are completely within the error. Even in the slope down rate, the curves are similar, presenting more consistent results compared to the literature (Wang et al, 2013; Farias et al., 2022). The maximum error in the peak temperature was approximately 5%.

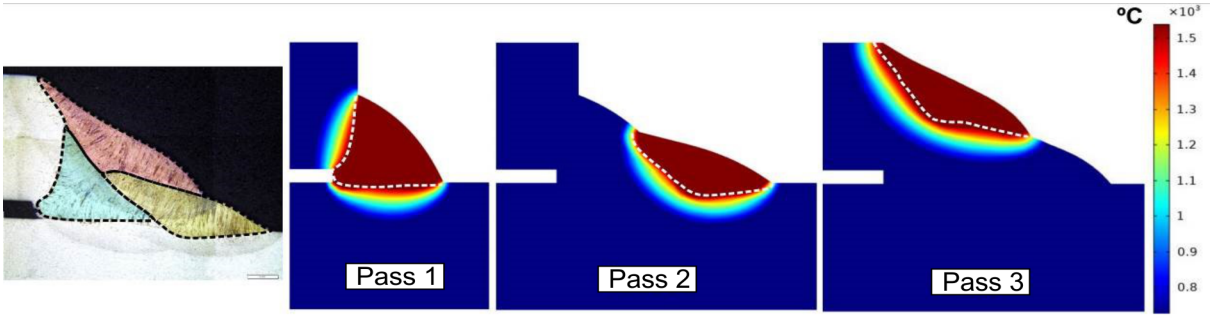

Fig. 6. Comparison of experimental macrography versus simulated weld bead (cross-section) for the condition without pre-heating.

RESULTS AND DISCUSSION

FEA analysis and validation of the model based on experimental results

Fig. 6 presents a comparison between the macrography of the welding without induction heating versus the simulated molten zone of the numerical analysis. In the image, the outer surface of the sleeve is the upper edge of the simulated cross-section. The contour of the experimental weld passes (black dashed lines) closely matches the FEA weld passes (white dashed lines), showing a good adjustment of the simulation conditions and the applied double-ellipsoidal heat source. Measuring the molten zone area of macrography and comparing it with the calculated ones, the error was 7.2 %, 7.0 %, and 6.2% for passes 1, 2, and 3, respectively. Therefore, the average error was 6.9 % in area, which is an excellent approximation based on other literature simulations (Bang et al., 2002; Nolan et al., 2005).

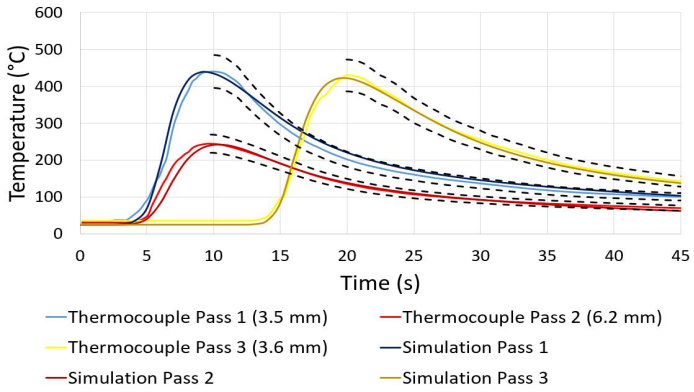

Fig. 7. Comparison of experimental thermal cycles versus the simulation probes (dashed lines represent an error of ±10% around the experimental thermal cycle).

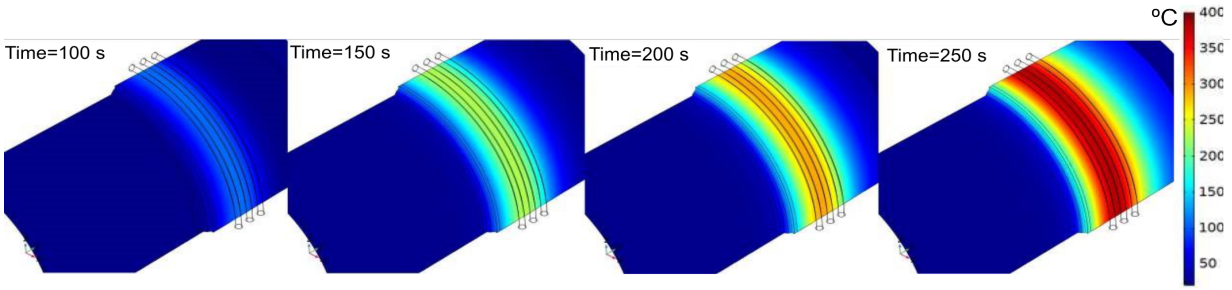

Fig. 8. Transient temperature analysis of the induction preheating

The errors verified in the comparison of the molten zone and thermal cycles were assumed as acceptable and sufficiently low to follow with the next steps of the model. After the validation of the model and the matching between experimental results (molten zone and thermal cycles), induction preheating was implemented. Fig. 8 represents an isometric view of the transient FEA calculated before the welding simulation. In this step, only the induction is considered in the model rising up the initial temperature up to the pre-defined level. The time steps show the temperature rising in the sleeve domain and in the pipe wall, in which a maximum of 400 ºC was delimited in the part.

From Fig. 9 it is possible to interpret the phenomenon acting on the part and even the temperature behavior for each three passes at the pipe wall. Preheating level for each pass is described in the figure's caption. Before the welding of the first pass, the coil set around the sleeve does not contribute efficiently to the temperature rising in the pipe wall. This is due to the fact that heat is exchanged between the sleeve and the pipe wall mostly by radiation and convection due to the existence of an air gap between both parts. After the deposition of the first pass, before the second one, a connection is created between the sleeve and the pipe providing the condition for conduction heat flux. The same can be stated for the third pass, which is also affected by the higher temperatures in the sleeve. From this FEA it can be verified that the most critical zone of the welding is the weld's toe, where higher cooling rates are faced due to the lower pre-heating temperature. This behavior and its consequences are going to be explained further in this work. The preheating temperature hit in the weld's toe for each weld bead (1, 2, and 3) was 60 ºC,90 ºC, and 100 ºC in this first test condition (induction power source set to 35 kW).

On the post-processing evaluation of Fig.10, the comparison of the macrography, for preheated weld bead with simulated molten zones showed an excellent agreement. Area measurements resulted in 9.6%, 11.6%, and 13.2% of errors in passes 1, 2, and 3, respectively. The average error was then 11.4%. This value was 4.5% higher than the condition without preheating. The reason for the increase in the error can be the initial temperature distribution, which can be slightly different around the pipe circumference. For example, in the real welded pipe, the position of the coil to the joint and its settlement around the part can vary. Even small differences in the experimental assembly, compared with the ideal model, can change the initial condition. Also, at some point underneath the sleeve (in the air gap), there may be contact between the sleeve and the pipe wall, and heat can be transferred by conduction assisting the initial temperature rise. Even though some experimental effects are difficult to be accounted for, and the strong multiphysics present in the in-service welding, the error obtained was relatively low and acceptable compared to results in the literature (Knoedel et al., 2017).

The relatively low error in the temperature distribution of the molten zone can be also verified in the thermal cycle curves. The slope down of the lines fitted within the 10% threshold, as can be seen in Fig. 11. Thus, the cooling rate estimated by FEA can represent the real value from the experimental trials.

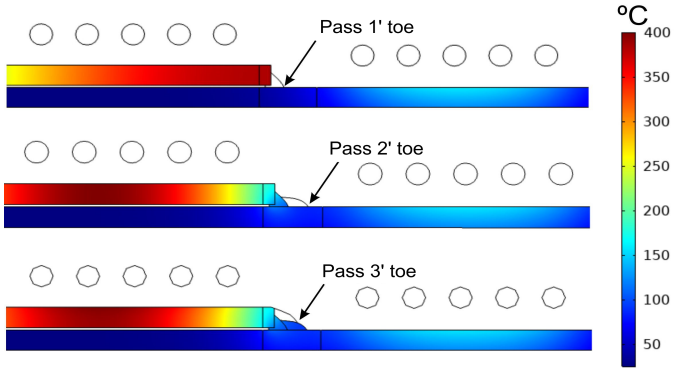

Fig. 9. Preheating simulation (1- 60 ºC, 2- 90 ºC, and 3- 100 ºC) and temperature distribution in the pipe and sleeve wall before the deposition of each weld bead.

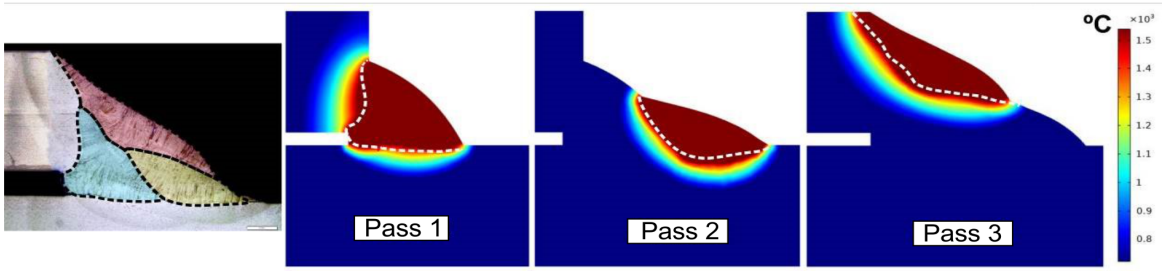

Fig. 10. Simulation of preheated condition (1- 60 ºC, 2- 90 ºC, and 3- 100 ºC) and comparison of experimental macrography versus simulated weld bead.

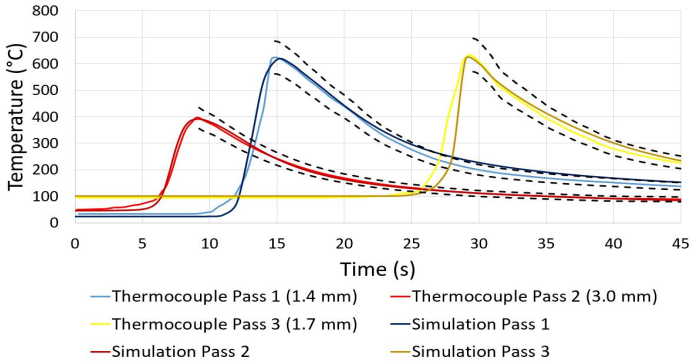

Fig. 11. Simulation of preheated condition (1- 60 ºC, 2- 90 ºC, and 3- 100 ºC) and comparison of the experimental and simulated thermal cycles for GMAW-P welding (dashed lines represent an error of ±10% around the experimental thermal cycle)

Weld bead cooling rate and microstructure evaluation

Due to practical issues and limitations that impede the measurement near the arc, it was not possible to measure the Δt_{8-5} direct with thermocouples, as indicated by the peak temperatures in Fig. 7 and Fig. 11. The modeling probes can be trustily positioned at any desired point of the domain and the cooling time get from post-processing step. Thus, the simulation becomes a valuable method for the estimation of cooling rates. The greater temperature gradient in high-cooling rate applications also difficult the measurement of high peak temperatures (e.g. above 800 ºC). In-service welding has hundreds of ºC per mm (Riffel, 2022).

Thus, Table 3 presents the Δt_{8-5} estimated for the conditions without and with induction heating tested in this work. As also mentioned in the last section of this paper, the faster cooling rate identified in this application was in the second weld bead's toe. For the condition without preheating the Δt_{8-5} at this point was 3.0 s (100 ºC/s), 0.2 s faster than the first pass, and 1.6 s faster than the third pass. Preheating the part at the temperatures indicated in Table 2, the cooling rate was reduced, but the faster condition was also in the second pass' toe with 3.9 s. Preheating the part provided more effect on reducing the cooling rate for passes 1 and 3. According to the welding sequence, these passes melt the sleeve which is at a high temperature (set to 400 ºC) and the effect of the initial temperature elevation is then more significant. Even though the initial preheating of the second pass's toe stayed in the neighborhood of 100 ºC, slightly affecting the Δt_{8-5}, this value has a great effect on the reduction of hydrogen content by enhancing its diffusion coefficient. Literature shows that from 20 ºC to 100 ºC the hydrogen diffusivity increases by about 1000X (Lippold, 2014).

Table 3. Δt8-5 and cooling rate for tested conditions

Δt8-5 (s) – Cooling rate (°C/s)			
Pass	No preheating	Preheating temperature (Weld bead's toe)	Preheated
1	3.2 - 93	60 ºC	4.9 - 61
2	3.0 - 100	90 ºC	3.9 - 76
3	4.6 - 65	100 ºC	5.6 - 53

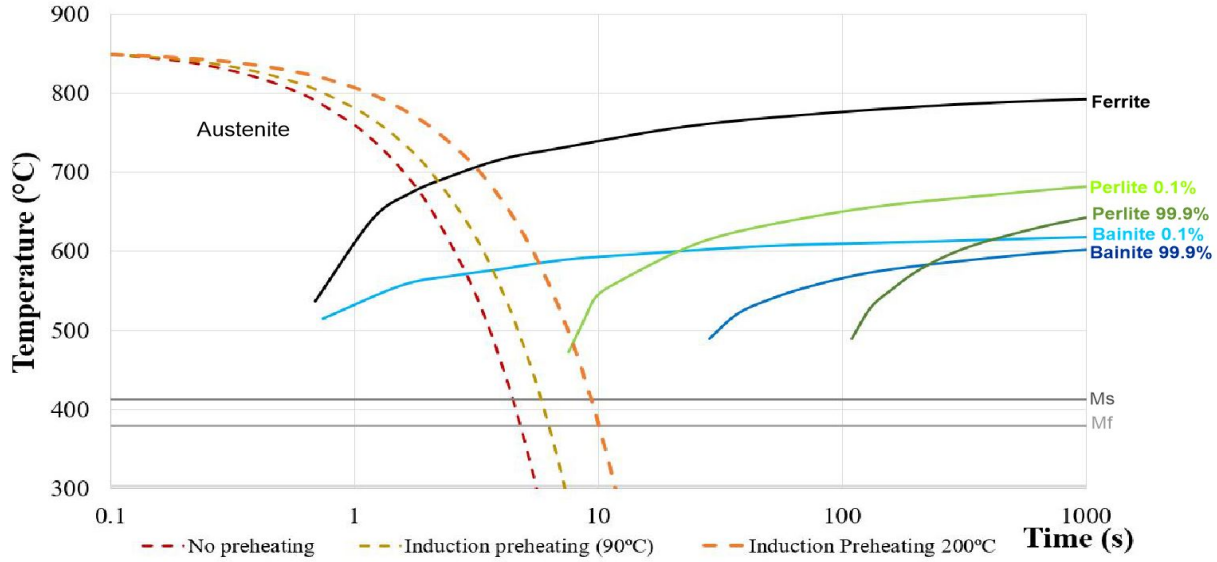

Fig. 12. CCT diagram plotted with cooling rate curves for conditions without preheating and with induction preheating.

The second pass also suffers more influence from the convective heat flux inside the pipe and lower temperatures are expected at this point. Thus, a higher preheating temperature was tested only at the second pass. For that, the maximum power of the induction source (60 kW) was applied. In such conditions, the temperature reached in the pipe wall surface (second pass' toe) was 200 ºC. At this temperature, the Δt_{8-5} of the second weld bead increased to 5.5 s (54 ºC/s) about half of the cooling rate at lower temperatures.

The effect and microstructure precipitation can be predicted using the continuous cooling transformation (CCT) diagram of the API 5L Grade B. The diagram calculated using the JMat Pro software and with its chemical composition as boundary condition is presented

in Fig. 12. Plotting the cooling rate, for the conditions of the most critical cooling rate (second pass), over the CCT it is possible to verify that for conditions without preheating the microstructure in the pass' toe is formed by ferrite, bainite, and martensite. Increasing the initial temperature to 90 ºC in the second pass' toe, the cooling rate reduced from 100 ºC/s to 76 ºC/s, but the microstructure slightly changed, and it is still formed by ferrite, bainite, and martensite. Enhancing the initial value to 200 ºC, the cooling rate was much slower (54 ºC) and in that case, the cooling curve touched the perlite initiation curve. In other words, this change in the path of the cooling curve indicates the precipitation of a more ductile microstructure.

Table 4 presents HV10 hardness measurements for all welded conditions. In the case without preheating, the average hardness was 288.6 HV and the maximum was 310.2 HV. With induction preheating at lower values (90 ºC at the second pass' toe) the maximum hardness measured was slightly reduced to 303.7 HV. On the other hand, when the initial temperature was increased to 200 ºC the maximum hardness dropped to 216.0 HV, a reduction of 87.7 HV. Such a great reduction of the property indicates a change in the microstructure of the welded sample, as pointed out in the CCT of Fig. 12.

Firstly, from the process point of view, it is important to mention that the weld beads did not present any defects, as it is possible to verify in the macrographies of Fig. 13. The condition with 200 ºC presented a deeper penetration in the pipe's wall due to the extra heat input provided by the induction. A greater wettability was also verified in the conditions with preheating, although in the macrographies such an aspect is not so clear.

Comparing the microstructures in the point with the higher hardness (second pass's toe) of each pass it was possible to verify a great difference in the morphology. Fig 14 shows a mostly martensitic (M) microstructure in the case without preheating and a very fine grain boundary ferrite (GBF). The same can be observed in the case with 90 ºC, in which is also possible to verify bainitic (FS(B)) regions. However, in the case of 200 ºC, larger ferritic grains (GBF) can be seen in the structure, and a very small region with martensite (M) and bainite (FS(B)) is observed right near the fusion line. Such larger ferrite grains result from the long time that the microstructure stays at higher temperatures due to the reduction of the $\Delta t_{8\text{-}5}$, enabling carbon diffusion.

Table 4. HV10 hardness values for welded samples.

Condition	No preheating	Preheating	
		90 ºC	200 ºC
Indentations	310.9	250.5	216.0
	302.7	303.7	203.3
	310.2	274.1	190.5
	307.4	264.3	188.0
	295.5	261.4	184.5
Average	288.6±36	264.6±19	190.5

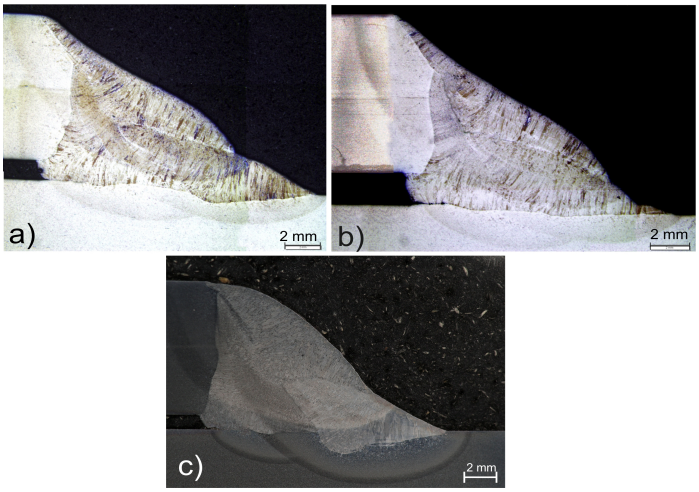

Fig.13. Macrographies of the welding beads, In a) No preheating; b) With induction preheating in passes 1, 2, and 3 (60 ºC, 90 ºC, and 100 ºC); c) With 200 ºC at each pass's toe.

CONCLUSIONS

The present work showed an analysis of different aspects of in-service welding, approaching FEA, and experimental results. The main conclusions of this work can be resumed as follows:

- A validation of a FEA for in-service welding was successfully reached based on the comparison of the experimental weld metal and the simulated molten zone, following a second criterion which was the low error in comparing experimental thermal cycles versus the simulated ones;
- Induction preheating was able to hit temperatures above those found in the literature for in-service with conventional methods (flame and electric resistance). The maximum value hit with 60 kW in this work was 200 ºC at the weld's toe;
- A great difference was verified in the microstructure comparing the case without preheating versus the intermedium temperature and the 200 ºC. The maximum hardness was 310.9 HV, 303.7 HV, and 216.0 HV, respectively;
- Using the CCT diagram plotted with the cooling rate curves it was possible to estimate the microstructure of the welded samples. The higher the initial temperature, the larger the ferrite amount, and the more ductile was the microstructure.

ACKNOWLEDGEMENTS

The authors would like to acknowledge the LABSOLDA staff for their technical support. In the same way, the authors appreciate the funding support of Petrobras, UFSC POSMEC, and the Brazilian Council for Scientific and Technological Development (CNPQ).

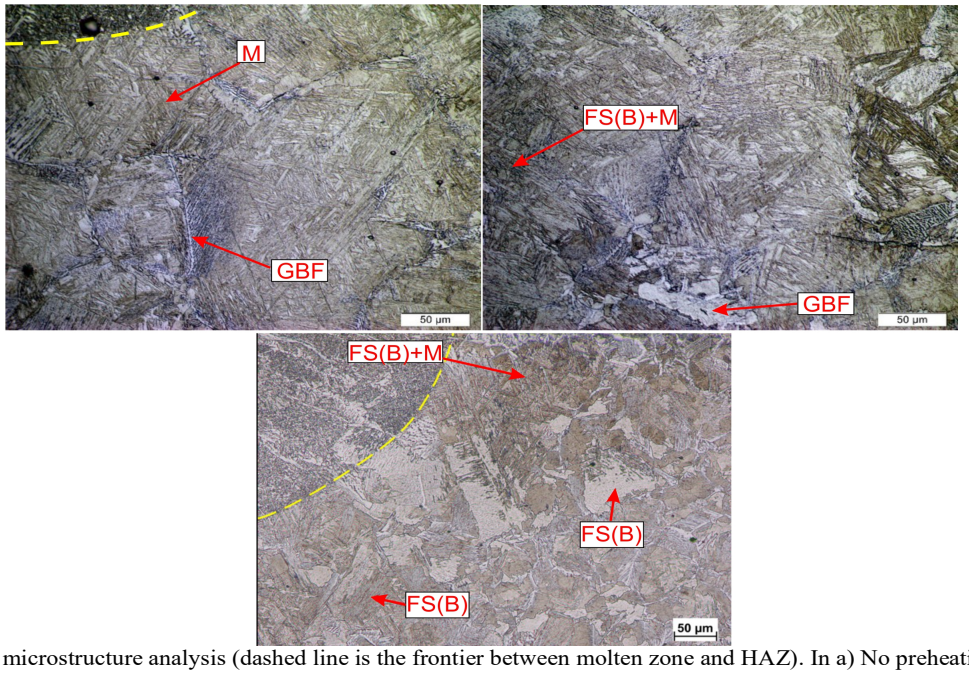

Fig. 14. Second pass' toe microstructure analysis (dashed line is the frontier between molten zone and HAZ). In a) No preheating; b) 90 ºC; c) 200 ºC.

REFERENCES

Ahmed, RA.; Shazly, M.; Megahed.MM (2016). 3D Finite Element Modeling of In-Service Sleeve Repair Welding of Gas Pipelines. International Journal of Pressure Vessels and Piping, Volume 146, Pages 216-229.

API 1104 (2007). The standard for Welding Pipe Lines and Related Facilities. American Petroleum Institute, USA. 50 p.

ASTM E384-17 (2021). Standard Test Method for Microindentation Hardness of Materials. ASTM International.

Bang, IW.; Son, YP.; Oh, KH.; Kim, YP.; Kim, WS. (2002). Numerical Simulation of Sleeve Repair Welding of In-service Gas Pipelines. Welding Journal: 273-82.

Boring, MA; Bruce, WA. (2008) The Effect of Hoop Stress on the Burnthrough Susceptibility During In-service Welding of Thin-Walled Pipelines. Proceedings of 7th International Pipeline Conference. September 29 – October 3, 2008. Calgary, Alberta, Canada.

Bosworth, MR. (1991). Effective Heat Input in Pulsed Current Gas Metal Arc Welding with Solid Wire Electrodes. Welding Journal (5), 111s-117s.

Bruce, WA. (2002). Qualification of Procedures for Welding onto In-Service Pipelines. Proceedings of the 4th International Pipeline Conference. Calgary, Alberta, Canada. September 29 – October 3, 2002. pp. 39-53. ASME.

Bruce, WA.; Bradley, CE. (2012) "Further Development of Heat-Affecter Zone Hardness Limits for In-service Welding". Proceedings of the 2012 9th International Pipeline Conference. September 24-28, Calgary, Alberta Canada.

Christensen, N.; Davies, V.; Gjermundsen, K. (1995). The Distribution of Temperature in Arc. British Welding Journal, v. 12(2), 54 p – 75 p.

Dutra, JC.; Silva, RHG.; Savi, BM.; Marques, C.; Alarcon, OE. (2016). New Methodology for AC-pulsed GMAW Parameterization Applied to Aluminum Shipbuilding. Journal of the Brazilian Society of Mechanical Sciences and Engineering volume 38, pp 99–107.

Farias, RM.; Teixeira, PRF.; Vilarinho, LO. (2022). Variable Profile Heat Source Models for Numerical Simulations of Arc Welding Processes. International Journal of Thermal Sciences, Volume 179, 107593.

Goldak, J.; Chakravarti, A.; Bibby, M. (1984). New Finite Element Model for Welding Heat Sources. Metallurgical Transactions B, v.15B, 299 p – 305 p.

Goldak, JA.; Akhlaghi, M. (2005) Computational Welding Mechanics.

Guest, S; Dyck, J; Egbewande, A; Mackenzie, R; Sadowski, M. (2016) Design of in-Service Repair Welding Procedures for Operating Pipelines: Critical Assessment of Variables Affecting Restraint Level and Heat-Affected Zone Microstructures of Vintage Pipelines. Proceedings of the 2016 11th International Pipeline Conference. September 26-30, Calgary, Alberta, Canada.

IMC Soldagem. SAP V4 DUPLO. Available on: https://www.imc-soldagem.com.br/pt-br/equipamentos/sistemas-de-monitoramento/sap-v4ti.

Joseph, A.; Harwig, D.; Farson, DF.; Richardson, R. (2003) Measurement and Calculation of Arc Power and Heat Transfer Efficiency in Pulsed Gas Metal Arc Welding. Science and Technology of Welding and Joining, vol 8 (6).

Kiefner, JF., Fischer, RD., Mishler, HW. (1981) Development of Guidelines for Repair and Hot Tap Welding on Pressurized Pipelines.

Final Report – Phase 1. Repair and Hot Tal Welding Group. Battelle Columbus Laboratories.

Kiefner, JF., Barnes, CR., Gertler, RC., Fischer, RD., Minshler, HW. (1983). Experimental Verification of Hot Tap Welding Thermal Analysis. Final Report – Phase II – Volume 2, Liquid Propane Experiments. Repair and Hot Tap Welding Group. Battelle Columbus Laboratories.

Knoedel, P.; Gkatzogiannis, S.; Ummenhofer, T. (2017). Practical Aspects of Welding Residual Stress Simulation. Journal of Constructional Steel Research. Volume 132, Pages 83-96.

Korol'kov, PM. (2012). Efficient Methods of Preheating in Welding Joints in Pipelines. Welding International, v. 26 (2), 155 p – 159 p.

Kou, S. Welding Metallurgy. (2003) Hoboken, NJ: Wiley-Interscience, p 411.

Lippold, JC. (2014). Welding Metallurgy and Weldability. John Wiley and Sons, Hoboken, New Jersey.

Nolan, D.; Sterjovski, Z.; Dunne, D. (2005). Hardness Prediction Models Based on HAZ Simulation for in-service Welded Pipeline Steels. Science and Technology of Welding and Joining, v.10, n.6, p. 681-694.

Palani, PK.; Murugan, N. (2006) Selection of Parameters of Pulsed Current Gas Metal Arc Welding. Journal of Materials Processing Technology, vol. 172 (1), pp. 1-10.

Riffel, KC. (2022) Análise Experimental e Numérica da Soldagem em Operação Utilizando Gmaw-P DC/AC Assistida por Aquecimento por Indução. 260 p. Tese de doutorado - Curso de Engenharia Mecânica, Universidade Federal de Santa Catarina.

Sabapathy, PN; Wahab, MA; Painter, MJ. (2000) The Prediction of Burn-through During In-service Welding of Gas Pipelines. International Journal of Pressure Vessels and Piping 77. 669 p – 677 p.

Yunovich, M.; Thompson, NG. (2005) Evaluation of Preheat Requirements for In-service Welding. Technical Report to Pipeline Research Council International. Edison Welding Institute, July 5, Ohio, USA.

Wang, Y.; Wang, L.; Di, X.; Shi, Y.; Bao, X.; Gao, X. (2013) Simulation and Analysis of Temperature Field for In-Service Multi-Pass Welding of a Sleeve Fillet Weld. Computational Materials Science, volume 68, Pages 198-205.